Check for updates

AGU ADVANCING EARTH AND SPACE SCIENCES

Geophysical Research Letters

RESEARCH LETTER
10.1029/2025GL117459

Zeeman: A Deep Learning Framework for Regional Atmospheric Chemistry Forecasting

Mijie Pang[1], Jianbing Jin[2], Arjo Segers[3], Hai Xiang Lin[1,4], Guoqiang Wang[5], Hong Liao[2], and Wei Han[6]

[1]Delft Institute of Applied Mathematics, Delft University of Technology, Delft, The Netherlands, [2]State Key Laboratory of Climate System Prediction and Risk Management, Jiangsu Key Laboratory of Atmospheric Environment Monitoring and Pollution Control, Jiangsu Collaborative Innovation Center of Atmospheric Environment and Equipment Technology, School of Environmental Science and Engineering, Nanjing University of Information Science and Technology, Nanjing, China, [3]TNO, Department of Climate, Air and Sustainability, Utrecht, The Netherlands, [4]Institute of Environment Sciences, Leiden University, Leiden, The Netherlands, [5]School of Mathematics, Physics and Statistics, Shanghai University of Engineering Science, Shanghai, China, [6]CMA Earth System Modeling and Prediction Centre, Chinese Meteorological Administration, Beijing, China

Abstract Atmospheric chemistry encapsulates the emission of various pollutants, the complex chemistry reactions, and the meteorology dominant transport, which form a dynamic system that governs air quality. While deep learning (DL) models have shown promise in capturing intricate patterns for forecasting individual atmospheric components—such as $PM_{2.5}$ and ozone—the critical interactions among multiple pollutants and the combined influence of emissions and meteorology are often overlook. This study introduces a DL-based framework–Zeeman for atmospheric chemistry forecasting. Our model effectively captures the nuanced relationships among these constituents and while achieving a 68.5-fold increase in computational speed compared to traditional numerical model. Evaluations demonstrate that our approach rivals numerical model, offering an efficient solution for atmospheric chemistry forecasting. In the future, this model could be further integrated with data assimilation techniques to facilitate efficient and accurate atmospheric emission estimation and concentration forecast.

Plain Language Summary In this paper, we created an atmospheric chemistry transport model called Zeeman that simulates air pollution concentration using advanced deep learning architecture. It looks at how pollution, weather, and emissions interact in regional scale on a hourly basis. We tested it and found it works well for pollutants like ozone and particles in the air, and it catches daily changes in more active pollutants like nitrogen dioxide. The model also tracks how pollution varies at different heights in the atmosphere. This is a notable improvement, though additional enhancements would be beneficial. Adding more details about how vertical diffusion, connecting pollution to weather changes, and using real-world observations could make it more accurate.

Key Points:

- By integrating concentration, emission, weather, and boundary fields, a deep learning regional atmospheric chemistry model is proposed
- Zeeman shows high correlations across spatial and vertical layers and stable 5-day simulations revealing daily patterns

Supporting Information:

Supporting Information may be found in the online version of this article.

Correspondence to:

J. Jin and W. Han,
jianbing.jin@nuist.edu.cn;
hanwei@cma.gov.cn

Citation:

Pang, M., Jin, J., Segers, A., Lin, H. X., Wang, G., Liao, H., & Han, W. (2026). Zeeman: A deep learning framework for regional atmospheric chemistry forecasting. *Geophysical Research Letters*, *53*, e2025GL117459. https://doi.org/10.1029/2025GL117459

Received 7 JUL 2025
Accepted 10 MAR 2026

© 2026. The Author(s).
This is an open access article under the terms of the Creative Commons Attribution-NonCommercial License, which permits use, distribution and reproduction in any medium, provided the original work is properly cited and is not used for commercial purposes.

1. Introduction

Atmospheric chemistry, a field that intertwines the subtle dance of emissions, concentrations, and meteorological patterns, stands as a vivid illustration of the intricate web of interactions within our environment. At its core, this discipline explores how pollutants and natural substances are emitted into the atmosphere, transform through chemical reactions, and are transported by the wind and other atmospheric processes (Sokhi et al., 2022). The complexity arises from the fact that these components do not operate in isolation; rather, they form a dynamic system where each element influences the others in profound ways. Emissions, originating from anthropogenic and natural sources, introduce diverse chemicals into the air, setting the stage for a series of chemical reactions (Xiao et al., 2021). These reactions, in turn, are heavily influenced by the prevailing meteorological conditions (Y. Qu et al., 2021), such as temperature and humidity (Su et al., 2020), which can either accelerate or decelerate reaction rates (Mu et al., 2018). Meanwhile, the concentration of these substances in the atmosphere, shaped by both emission rates and removal processes, plays a crucial role in determining the impact on air quality and climate (Raes et al., 2010). Understanding the interplay between emissions, concentrations, and meteorology is crucial for performing air quality forecasting and addressing pressing environmental challenges (X. Lu et al., 2019; Y. Zhang, 2008). Moreover, this understanding serves as the foundation for data assimilation and emission inversion, which are key focuses in atmospheric research (Zhu et al., 2023). While this interplay brings

19448007, 2026, 6, Downloaded from https://agupubs.onlinelibrary.wiley.com/doi/10.1029/2025GL117459 by Nanjing University Of Information Science & Technology, Wiley Online Library on [23/03/2026]. See the Terms and Conditions (https://onlinelibrary.wiley.com/terms-and-conditions) on Wiley Online Library for rules of use; OA articles are governed by the applicable Creative Commons License

Table 1
Overview of the Data Set

Category	Dimension	Dimension type	Species
Concentration	17 × 11 × 40 × 50	3D	no2, o3, co, so2, nh3, nh4a, pan, so4a, no3a_f, no3a_c, ec, pom, ppm, tnmvoc, tpm25, tpm10, tss
Meteorology3d	5 × 11 × 40 × 50	3D	t, rh, u, v, p
Meteorology2d	2 × 1 × 40 × 50	2D	blh, rain
Emission	27 × 1 × 40 × 50	2D	no2, no, co, form, ald, par, ole, eth, tol, xyl, so4a_f, so2, ch4, nh3, iso, terp, ec_f, ec_c, pom_f, pom_c, ppm_f, ppm_c, na_ff, na_f, na_ccc, na_cc, na_c
Boundary	17 × 11 × 2 × (40 + 50)	3D	Same as concentration

substantial computational demands and casts great challenges to efficiently consider the intricate dynamics of atmospheric chemistry (Feng et al., 2021). High demand of computation can be noticed especially when atmospheric chemistry is involved (Gao et al., 2024; Grell & Baklanov, 2011).

Deep learning (DL) models have demonstrated remarkable capabilities in processing and analyzing large amounts of data (Yu & Ma, 2021). These DL models can capture complex patterns and relationships within atmospheric conditions, providing precise and timely forecasts (Burgh-Day & Leeuwenburg, 2023). Numerous of researches have applied DL models to perform forecasts within different aspects of atmospheric chemistry (Méndez et al., 2023; Tang et al., 2024; B. Zhang et al., 2022). B. Zhang et al. (2020) proposed a model based on an autoencoder and bidirectional long-short term memory to predict the $PM_{2.5}$ concentration. $PM_{2.5}$ concentration, meteorological factors are used as inputs in this model. Cheng et al. (2022) combined a generative adversarial network with a variational autoencoder to learn the relationship between meteorological factors and ozone. Long lead-time ozone predictions can be made by this model. B. Lu et al. (2023) developed a space-time Light Gradient Boosting Machine model to estimate the spatial distribution of Non-methane volatile organic compounds (NMVOCs). The model incorporates NMVOCs station observations, satellite-derived emissions data, and meteorological information as inputs. The strong influence of emissions on NMVOCs estimation were emphasized. While these models exhibit relatively good performance in predictions, they are typically constrained to single component or combined indices, such as $PM_{2.5}$ and the Air Quality Index. Interplay between diverse components is often overlooked, limiting the models' comprehensiveness. For example, nitrogen oxides (NOx) and volatile organic compounds (VOCs) undergo a series of complex chemical reactions under sunlight, leading to the formation of O_3 (George et al., 2015). Precursor substances like sulfur oxides (SOx), nitrogen oxides (NOx), and ammonia (NH_3) can transform into secondary aerosols such as sulfates, nitrates, and ammonium salts which constitute $PM_{2.5}$ through various chemical reactions in the atmosphere (Peng et al., 2021). These components are closely related to each other, and their interactions are essential for building the atmospheric chemistry transport model. Furthermore, emissions and meteorology play an crucial role in determining the increase or decrease of concentrations. Relative humidity (RH) has a substantial impact on the evolution of secondary aerosol in the atmosphere (Ma et al., 2021). Surface ozone can be effected by boundary layer height (blh) in a complex way (C. Zhang et al., 2023). On the other hand, emissions are the major source of air pollution (S. Li et al., 2023). While emissions are frequently overlooked when designing a DL based prediction model due to difficulties in acquiring high spatio-temporal resolution information. In general, meteorological fields and emissions are inherently integrated with atmospheric concentration levels (J. Wang et al., 2024). To achieve an accurate air quality prediction, incorporation of both elements is necessary. Nevertheless, their complex dynamics also present significant challenges to modeling efforts.

In recent years, the integration of DL methodologies into weather prediction has inaugurated a new epoch characterized by unprecedented levels of accuracy and computational efficiency (Bi et al., 2023; Chen et al., 2023; Lam et al., 2023). These advancements, collectively termed artificial intelligence (AI)-based approaches, have enabled models to discern intricate patterns within atmospheric dynamics, thereby offering superior forecast precision and timeliness compared to conventional numerical weather prediction techniques (Charlton-Perez et al., 2024). This study introduces an advanced DL driven framework for atmospheric chemistry transport - Zeeman. Our contributions are twofold: Comprehensive Multi-Pollutant Simulation: We expand the scope of atmospheric chemistry components to encompass O_3, NH_3, NO_2, fine particulate matter ($PM_{2.5}$), and coarse particulate matter (PM_{10}). A detailed inventory of these components is provided in Table 1. By employing

19448007, 2026, 6, Downloaded from https://agupubs.onlinelibrary.wiley.com/doi/10.1029/2025GL117459 by Nanjing University Of Information Science & Technology, Wiley Online Library on [23/03/2026]. See the Terms and Conditions (https://onlinelibrary.wiley.com/terms-and-conditions) on Wiley Online Library for rules of use; OA articles are governed by the applicable Creative Commons License

an attention mechanism, our model adeptly captures the nuanced interactions among these constituents, achieving performance metrics that rival those of numerical model across main components. Enhanced Framework via Integrated Data Streams: The efficacy of our model is further improved by the incorporation of hourly meteorological data alongside emissions. Given the pivotal role of both meteorological parameters and emission sources in determining atmospheric concentrations, this enriched data set facilitates the generation of stable predictions with extended lead times (Y. Zhang et al., 2012). In addition, Zeeman is a regional model whose forecast can be impacted by external inputs. Therefore, the boundary conditions are also considered in Zeeman.

While the study primarily focuses on designing a fast, surrogate model that approximates LOTOS-EUROS, its applications extend well beyond this. For example, Zeeman can be off-line integrated into meteorological models to provide coupled forecasts. Data assimilation can be implemented using Zeeman through variational or ensemble methods, providing a framework that delivers greater accuracy and efficiency (Y. Li et al., 2024; W. Wang et al., 2024; Zhong et al., 2024).

This paper is organized as follows: Section 2 introduces the data set used to train the model. Section 3 introduces the overall architecture of Zeeman and training details. Section 4 evaluates the performance of Zeeman forecasts in terms of series metric, spatial, vertical aspects. In the end, Section 5 concludes the paper and point out limitations and future work.

2. Data Set

This section introduces all the data used to train the Zeeman including 3D concentrations from LOTOS-EUROS simulations, emission, meteorological fields and boundary conditions. These emission, meteorology and boundary fields are also driving LOTOS-EUROS model to produce concentration simulations. The data set spans the period from 2018 to 2022. The first four years (2018–2021) are used for training the model and the last year, 2022, is reserved for evaluating model performance.

2.1. LOTOS-EUROS Simulations

We used the open-source CTM LOTOS-EUROS v2.2, a three-dimensional (3D) regional chemistry transport model for simulation of trace gases and aerosol concentrations (Manders et al., 2017; TNO, 2025). It has been wildly used for air quality researches and forecasting (Skoulidou et al., 2021; Timmermans et al., 2017, 2022). LOTOS-EUROS constitutes one of the state-of-the-art atmospheric chemistry models used by the Copernicus Atmosphere Monitoring Service (Colette et al., 2024) to provide daily forecasts of the main air pollutants, that is, O_3, NO_2 and PM_{10}.

2.2. Simulated Concentrations

In this study, 3D concentration are generated by the LOTOS-EUROS for the main air pollutants. These include trace gases such O_3, NOx, NH_3, carbon monoxide (CO), and NMVOC, and aerosols (particulate mater) of various types for size bins within a range of 0–10 μm. A full model configuration has 54 transported tracers. For the Zeeman model, a limited set of 17 tracers is used which are either one of the original tracers, or an accumulated tracer such as total $PM_{2.5}$ and PM_{10} (all particulate matter with diameters less than 2.5 or 10 μm). The full list of selected concentrations is detailed in Table 1.

2.3. Model Domain and Resolution

The model domain is limited to an area over Netherlands, illustrated in Figure S23 in Supporting Information S1. Simulations in this domain are at a resolution of $0.1° \times 0.1°$, which is the same as the operational resolution in the CAMS forecast. For the chosen domain, the model simulates concentrations at 50×40 grid cells of approximately 10×5 km wide. In the vertical, 11 layers are used that are a coarsening of the ECMWF operational meteorological data described below; the lowest layer is about 20 m thick, and the top is around 9 km.

2.4. Boundary Conditions

For a regional atmospheric chemistry model, boundary conditions plays an important role especially after lone time forecasting (K. Qu et al., 2024). Then boundary conditions of concentration is then included in Zeeman. The boundary conditions for the European run are obtained from the CAMS near-real-time global chemistry

19448007, 2026, 6, Downloaded from https://agupubs.onlinelibrary.wiley.com/doi/10.1029/2025GL117459 by Nanjing University Of Information Science & Technology, Wiley Online Library on [23/03/2026]. See the Terms and Conditions (https://onlinelibrary.wiley.com/terms-and-conditions) on Wiley Online Library for rules of use; OA articles are governed by the applicable Creative Commons License

simulations (Peuch et al., 2022). The simulations from the European domain are used as boundary conditions for the high-resolution simulation at the target domain, where all 54 tracers of the full model are transferred. The Zeeman model is however trained using the boundary values for the 17 selected (accumulated) tracers, obtained from the 1-layer shell of grid cells around the target domain. Experiment on the necessity of including boundary conditions is shown in Section 6 in Supporting Information S1.

2.5. Emission

This study employs the emission inventory from the Copernicus Atmosphere Monitoring Service REGional inventory (CAMS-REG) (Kuenen et al., 2021, 2022), a specialized data set designed to facilitate air quality modeling. CAMS-REG provides anthropogenic emissions data for Europe, starting from 2020, at a spatial resolution of $0.05° \times 0.1°$. The inventory encompasses a range of substances, including both air quality pollutants and greenhouse gases. For this work, we have selected the air pollutants, which includes emissions of nitrogen oxides (NOx), sulfur dioxide (SO_2), NMVOCs, ammonia (NH_3), carbon monoxide (CO), components of particulate matter(PM_{10}), as well as methane (CH_4). A comprehensive list of the species utilized in this work is detailed in Table 1. Full name of the emission can be found in Table S1 in Supporting Information S1. Note that the emissions at time t is the averaged emissions between t and $t + 1$. This one-step ahead strategy is adopted help model better characterize the impact of emissions to the future concentration states. All the emissions here are the combined value from anthropogenic and biogenic source.

2.6. Meteorology Data

Meteorology data is from ECMWF operational forecasts over 0–12 hr. Three-dimensitional (3D) variables including temperature (t), pressure (p), wind speed (uv_u, uv_v) and relative humidity (rh) are used as the input of training. Besides, 2D information of boundary layer height (blh), rain is also included in the training. These data are spatial-temporal interpolated to model grids. Time t of this data implies the instant values for the middle of the hour.

3. Methodology

This section introduces the overall architecture of the Zeeman including the architecture and training details. And the forecast strategy of Zeeman.

3.1. Model Architecture

The architecture of Zeeman consists of four main components, which are illustrated in Figure 1: boundary enhancement, cube embedding, Transformer blocks, and an output layer.

In the context of regional prediction models, boundary conditions play a crucial role, particularly for forecasts with longer lead times. Given that these models are predominantly influenced by wind patterns, there is a potential for concentrations outside the domain to be introduced into the area, which can result in underestimations of concentration if neglected. To address this issue, three-dimensional boundary values have been incorporated into the original concentration fields. This enhancement aims to provide a more accurate representation of concentration levels by accounting for external influences that may affect the region over longer forecast periods. A detailed description on boundary enhancement can be found in Section 4 in Supporting Information S1. Afterward, the space-time cube embedding is applied. The input data combines 3D, multi-component variables with dimensions of $T \times S_{in} \times H \times W$ and creates a data cube with dimensions of $H \times W \times C$, where T, S_{in}, H, and W represent the number of time steps, input channels containing all species on all levels, height, latitude and longitude grid points, respectively. C, the width of features, is set to be 1,800. Data from two time steps ($t-1$, t) are embedded into 1 layer.

This data cube undergoes processing through a series of Swin Transformer V2 blocks, a variant of the Vision Transformer that has demonstrated remarkable performance across various computer vision tasks (Liu et al., 2021). The Swin Transformer innovatively applies self-attention mechanisms within localized windows and establishes cross-connections by shifted windows, significantly enhancing computational efficiency and effectiveness (To et al., 2024). Swin Transformer V2 builds upon these strengths and utilizes a residual post normalization and a log-spaced continuous position bias technique, refining them to achieve even superior results

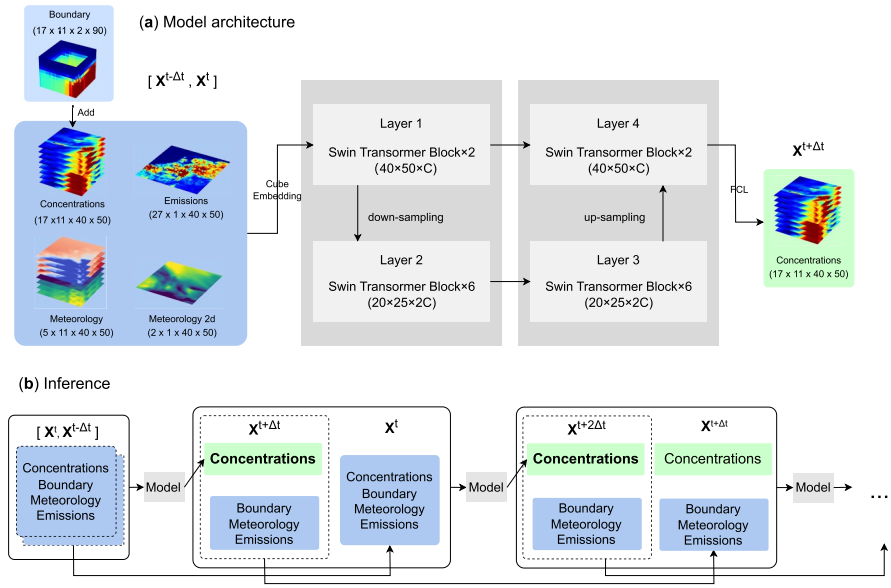

Figure 1. Overall architecture of Zeeman. (a) the main components of Zeeman: boundary enhancement, cube embedding, Swin-transformer, full connected layer. (b) the process of cyclic prediction based on Zeeman.

(Liu et al., 2022). The architecture is organized into layers as follows: In the first layer, the embedded data cube ($H \times W \times C$) is initially processed by two Swin Transformer blocks. Following the initial layer, a down-sampling module halves the horizontal dimensions while doubling the number of channels, transforming the data cube's dimensions to ($H/2 \times W/2 \times 2C$). The transformed data cube then passes through six Swin Transformer blocks, maintaining the dimensions of ($H/2 \times W/2 \times 2C$). The subsequent layers mirrors the structure of Layer 1 and Layer 2, maintaining the dimensions from Layer 2 and ultimately transits the data cube back to its original dimensions ($H \times W \times C$) after passing through an up-sampling module. A skip connection is established between Layer 1 and Layer 4, facilitating the concatenation along the feature channel for enriched feature representation. Lastly, a Fully Connected Layer projects the concatenated output to generate the final predictions. This structured approach ensures efficient and effective processing, culminating in refined output predictions. More details about the choices of model architecture can be found in Section 4 in Supporting Information S1.

3.2. Model Training

This section describes the training details for Zeeman. The model is developed on the Pytorch framework. The model is trained with 100 epochs using a batch size of 1 on each GPU. Training of the model took 100 hr on 4 Nvidia H100 GPUs. To accelerate the training process, Distributed Data Parallel is utilized (S. Li et al., 2020). Furthermore, to expedite data loading operations, the entire data set is loaded into the memory of main process and distributed to worker processes during training by the main process. The AdamW (Loshchilov & Hutter, 2019) optimizer is applied with an initial learning rate of 1×10^{-4} and gradually annealed to 0 following the cosine schedule. A weight decay coefficient of 0.1 is set. To alleviate risk of over-fitting, the samples are shuffled in each epoch. The training data includes hourly fields spanning from 2018 to 2021 (35,038 samples in total) and data in 2022 serves as the test data set (8,735 samples in total). Experiment showcasing the necessity of the length of data set is presented in Section 13 in Supporting Information S1.

The Mean Absolute Error loss is employed to supervise the training of the neural network. The loss function is defined as:

$$\mathcal{L} = \frac{1}{C \times H \times W} \sum_{i=1}^{C} \sum_{j=1}^{H} \sum_{k=1}^{W} \| \mathbf{f}_{i,j,k}(\mathbf{c}_{t+1}; \mathbf{c}, \mathbf{w}, \mathbf{e}, \mathbf{b}|_{t-1,t}) - \mathbf{y}_{i,j,k} \|^1 \quad (1)$$

19448007, 2026, 6, Downloaded from https://agupubs.onlinelibrary.wiley.com/doi/10.1029/2025GL117459 by Nanjing University Of Information Science & Technology, Wiley Online Library on [23/03/2026]. See the Terms and Conditions (https://onlinelibrary.wiley.com/terms-and-conditions) on Wiley Online Library for rules of use; OA articles are governed by the applicable Creative Commons License

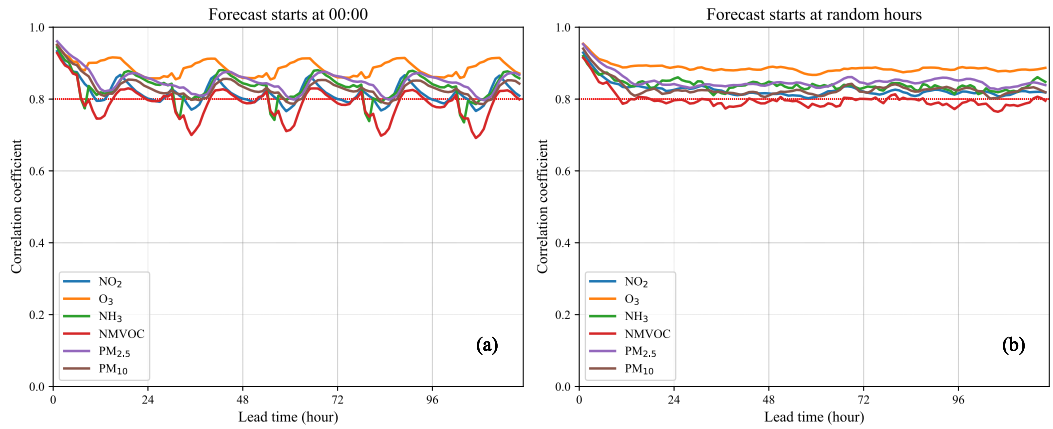

Figure 2. Correlation coefficient (R) as a function of forecast lead time (1–120 hr) for the Zeeman model. The left panel (a) illustrates performance for forecasts initiated at 00:00 daily in 2022, while the right panel (b) displays performance for forecasts initiated at random hours daily over the same period. Only data on ground layer is considered here.

where C, H, W are the number of channels and grids in latitude and longitude, i, j, k are the indices for the channels, latitude and longitude. **c**, **w**, **e** and **b** represent concentration, weather conditions, emissions and boundaries, respectively. **f** is the Zeeman forward function. It takes the inputs at two time steps and then produces the concentration forecasts at next time step. **y** means the LOTOS-EUROS simulated concentrations, also the training target.

3.3. Inference Strategy

The inference approach of Zeeman employs an auto-regressive strategy, as illustrated in Figure 1b. Initially, Zeeman uses input data from the initial fields at two time steps ($t - 1$ and t) to generate for the subsequent time point ($t + 1$). Next, applying known emissions, meteorology, boundary conditions, and the forecasted concentration at $t + 1$, the model predicts the concentration at $t + 2$. This process enables cyclic forecasting by iteratively applying the same strategy. After 2 steps, Zeeman is relying on its internal state and external forces to produce forecasts, which is as same as numerical CTMs. Each iteration takes 80 ms on a Nvidia 4080 GPU (68.5 times faster than LOTOS-EUROS), which means it only takes less than 10 s to produce 5-day hourly forecasts. In this paper, all experiments for evaluation start at 00:00 each day in 2022 and last for 5 days. The start time setting follows the operational air quality forecast that initiates at several fixed hours of the day. In addition, experiment with random start time is also performed to evaluate the performance excluding the impact from start time. The corresponding metrics are calculated on these series of forecasts and the metrics used in this research are listed in Section 2 in Supporting Information S1.

4. Results

This section showcases the comprehensive performance of Zeeman. First, the trend of errors over 5-day forecast is demonstrated and reflects Zeeman's consistent reliability. Then illustrations of the spatial and vertical error distributions highlight the accuracy of the 3D forecasting outcomes.

4.1. Forecast Metrics Comparison

In this section, we evaluate the forecasting performance of Zeeman over lead time of 120 hr. In practical applications, forecasts exceeding this time may be biased due to inaccuracies in weather and boundary condition predictions. Two experiments are performed where a fixed start hour 00:00 and a random start hour in the day is decided. The forecast runs each day in 2022 and lasts 120 hr from the start hour.

Figure 2a presents the time series of the correlation coefficient (R) for six major pollutants at an hourly resolution with fixed start hour. The results reveal a fluctuating yet generally stable performance across these pollutants. Additional metrics, including NMB, NME, and RMSE, are provided in Figures S19–S21 in Supporting Information S1. O_3 shows the highest correlation, with R 0.85 across all lead times. Particulate matter ($PM_{2.5}$ and

19448007, 2026, 6, Downloaded from https://agupubs.onlinelibrary.wiley.com/doi/10.1029/2025GL117459 by Nanjing University Of Information Science & Technology, Wiley Online Library on [23/03/2026]. See the Terms and Conditions (https://onlinelibrary.wiley.com/terms-and-conditions) on Wiley Online Library for rules of use; OA articles are governed by the applicable Creative Commons License

10.1029/2025GL117459

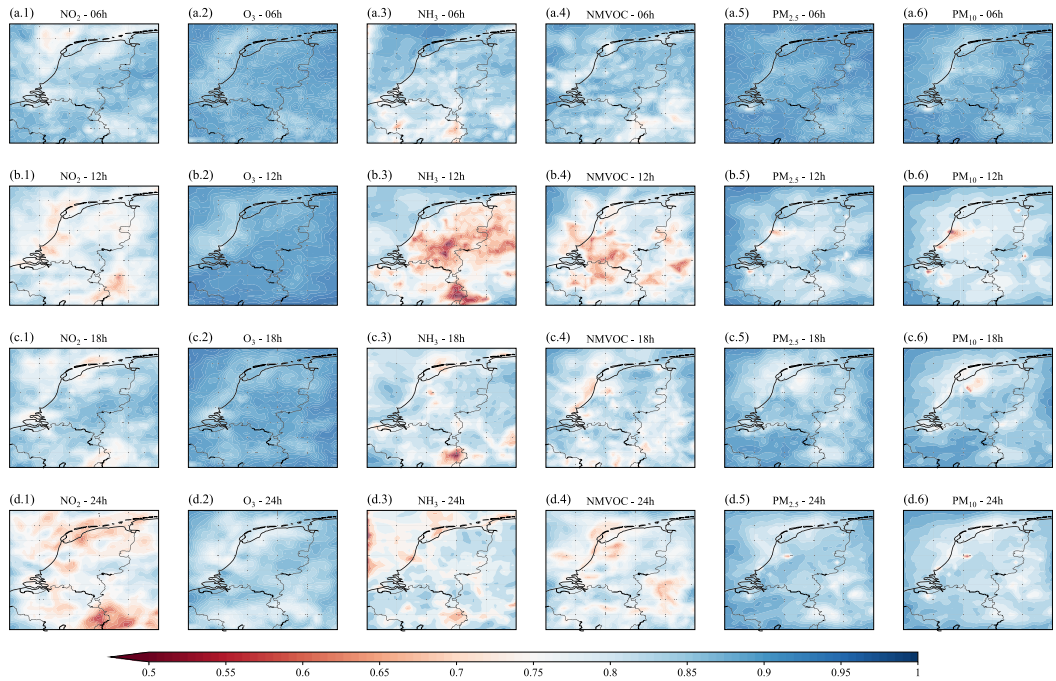

Figure 3. Spatial distribution of correlation coefficient (R) from Zeeman prediction and LOTOS-EUROS simulations for variables on ground level with the lead time of 6, 12, 18, 24 hr. All the predictions start from 00:00 at each day on 2022.

PM_{10}) follows similar trends, though performance for both dips around 14:00. This coincides with concentration minima driven by enhanced thermal advection and diffusion (Figure S4 in Supporting Information S1), which Zeeman partially struggles to capture. Similarly, performance for NO_2 and NH_3 reaches local minima at 12:00 and 06:00, respectively, aligning with their diurnal concentration troughs. NMVOCs exhibit the highest variation, R drops to 0.7 at 12:00 as photochemical consumption and inversion layer lifting reduce daytime concentrations. Overall, Zeeman's accuracy mirrors daily concentration cycles, showing slightly reduced consistency during peak daylight hours.

In general, there is a distinct daily periodic variation. For all displayed species, R begins at a high level but decreases over the first 12 hr, after which the periodic pattern stabilizes. This behavior reflects the transition between dominant drivers: short-term forecasts (<12 hr) are primarily governed by initial conditions and local emissions, whereas long-term forecasts (>12 hr) are dominated by the interplay of meteorology, boundary conditions, and daily emission cycles. The high correlation in the first 12 hr is largely attributable to the "memory" of the initial conditions. Once this influence fades, the model must rely on its ability to simulate complex meteorological-emission interactions, which poses a greater challenge. To isolate this effect, an experiment by initiating forecasts at randomized hours of the day is also conducted. As shown in Figure 2b, the trend becomes even more clear: R drops during the initial 12-hr predictions and remains stable thereafter, suggesting that error accumulation does not grow indefinitely but reaches a quasi-equilibrium governed by the quality of the forcing data. Marécal et al. (2015) compares the performance of several numerical atmospheric chemistry models within the lead time of 96 hr. Figure S22 in Supporting Information S1 illustrates a similar temporal variation trend, characterized by a recurrent "diurnal oscillation" in error metrics. It confirms that Zeeman isn't "drifting" or "exploding" as lead time increases; it is simply reacting to the varying difficulty of the atmospheric state.

4.2. Spatial Evaluation of Forecasts

Figure 3 illustrates the spatial distribution of the R derived from these forecast series. Forecasts with lead times of 6, 12, 18, and 24 hr were selected to highlight trends in error and variations between day and night. Meanwhile, these are also representative of the model's performance over subsequent days for the periodic pattern shown in

19448007, 2026, 6, Downloaded from https://agupubs.onlinelibrary.wiley.com/doi/10.1029/2025GL117459 by Nanjing University Of Information Science & Technology, Wiley Online Library on [23/03/2026]. See the Terms and Conditions (https://onlinelibrary.wiley.com/terms-and-conditions) on Wiley Online Library for rules of use; OA articles are governed by the applicable Creative Commons License

19448007, 2026, 6, Downloaded from https://agupubs.onlinelibrary.wiley.com/doi/10.1029/2025GL117459 by Nanjing University Of Information Science & Technology, Wiley Online Library on [23/03/2026]. See the Terms and Conditions (https://onlinelibrary.wiley.com/terms-and-conditions) on Wiley Online Library for rules of use; OA articles are governed by the applicable Creative Commons License

Section 4.1. The analysis includes major pollutants such as nitrogen dioxide (NO_2), ozone (O_3), ammonia (NH_3), NMVOCs (NMVOC), particulate matter less than 2.5 and 10 μm ($PM_{2.5}$ and PM_{10}).

The most outstanding performance is observed in the O_3 forecasts. As depicted in the second column of the figures, the correlation coefficient (R) for O_3 remains above 0.9 across most of the domain, even after 24 hr. Ozone, a secondary pollutant, is formed through complex chemical reactions involving precursor pollutants—primarily nitrogen oxides (NO_x) and VOCs—in the presence of sunlight. Meteorological factors, such as ambient temperature and humidity, also influence its formation. Boundary conditions also play an important role considering the longer life time of ozone. By jointly considering these factors, Zeeman gives good performance on O_3 forecast.

Forecasts for $PM_{2.5}$ and PM_{10} also demonstrate strong performance, with correlation coefficients (R) exceeding 0.85 across most domains. However, some regions exhibit noticeably lower values, particularly in (c.5) and (c.6). These anomalies are primarily linked to irregular fire emissions, which vary unpredictably in both time and location. Such events lead to rapid and extreme increases in pollutant concentrations over short periods, significantly degrading evaluation metrics. This effect is not limited to $PM_{2.5}$ and PM_{10} but is also observed in other species, such as NH_3 and NMVOC. A more detailed discussion of this phenomenon is provided in Section 10 in Supporting Information S1.

The performance of NO_2 forecasts varies across different hours. High correlation coefficients (R) are observed at 6 and 18 hr, while lower R values occur at 12 and 24 hr. The primary anthropogenic sources of NO_2 include the combustion of coal, oil, and gas in power plants, industrial facilities, and vehicles. As illustrated in Figure S1 in Supporting Information S1, NO_x emission trends reveal two distinct peaks around 08:00 and 16:00. Zeeman effectively adapts to these emission surges, achieving strong performance during these periods. At night, in the absence of photochemical reactions, NO_2 enters an accumulative phase. During this time, its variations are governed by reactions with O_3, as well as dispersion and mixing processes. The higher R values observed at night are attributed to an underestimation of concentrations, as evidenced in Figure S12 (a.4) in Supporting Information S1.

The performance of NH_3 forecasts exhibits significant variation across different hours. At 12:00, the correlation coefficient (R) distribution reaches its lowest point. This coincides with the combined effects of peak emissions (as shown in Figure S1 in Supporting Information S1) and enhanced dispersion driven by elevated temperatures, posing a challenge for the model to accurately capture both processes simultaneously. At other times, R remains relatively high and stable. Additionally, a notable shift in the differences between Zeeman and its low-emission variant is observed, as depicted in Figure S12 (c.4) in Supporting Information S1. During this period, emissions are low, and a lower inversion layer restricts dispersion, leading to NH_3 accumulation. This suggests that while Zeeman successfully captures the increasing trend of NH_3 at night, it may overestimate this effect.

The forecast for NMVOCs displays a trend comparable to that of NH_3. At 12:00, NMVOC emissions peak, contributing to elevated NH_3 levels. However, the accelerated rate of photochemical reactions consumes NH_3, while a higher inversion layer—driven by increased temperature and wind advection—adds further complexity to the dynamics. This interplay of factors challenges the model's ability to accurately capture the relationship, leading to diminished performance at noon. In contrast, at other times (06:00, 18:00, and 24:00), the model exhibits more consistent and stable performance.

Figure 4 shows the relationship between LOTOS-EUROS and Zeeman with lead time of 12 hr. To maintain visual clarity amidst the high volume of data, a random sampling strategy is employed, displaying only 1% of the total data points. The results demonstrate robust predictive accuracy, with R values exceeding 0.85 for the majority of species. The highest correlation was achieved for sea spray (0.948). This superior performance is likely due to the fact that sea spray emissions are primarily driven by stable physical parameters, such as surface wind speed over the ocean, which the DL model can easily map to the concentration output. In contrast, the lowest correlation was observed for sulfate (SO_4^{2-}). Unlike primary pollutants, sulfate is a secondary aerosol formed through complex non-linear chemical pathways. SO_4^{2-} is highly chemically active. Its formation involves multi-phase reactions (including aqueous-phase oxidation in clouds) that are highly sensitive to small fluctuations in humidity and precursor SO_2 concentrations. While DL models excel at capturing spatial transport, they often struggle to approximate the "stiff" numerical solvers used in chemical mechanisms, where a small change in environmental conditions can lead to a drastic shift in sulfate production rates.

10.1029/2025GL117459

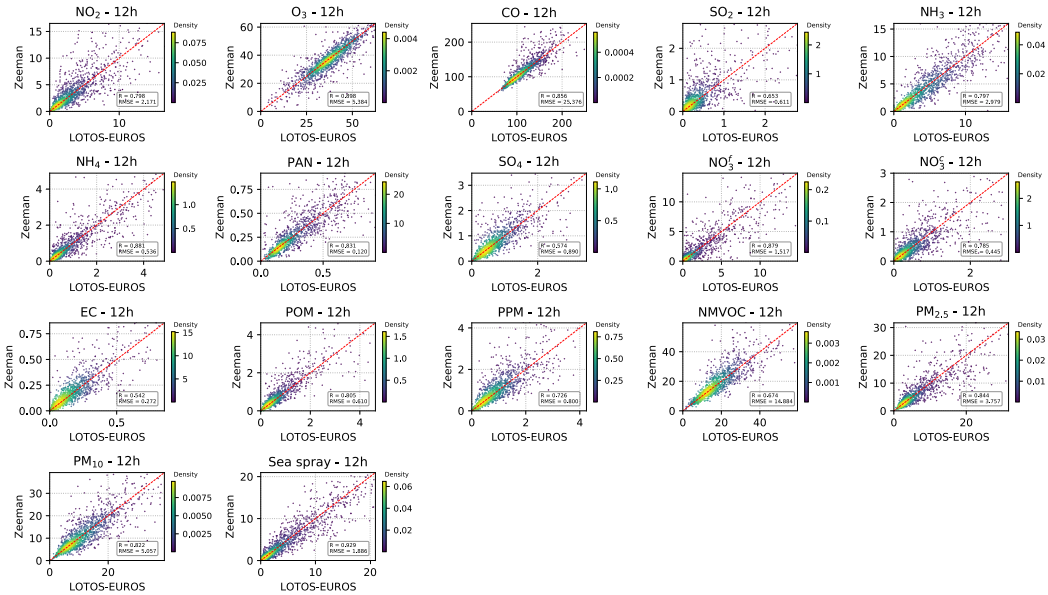

Figure 4. Density scatter plot of forecast of 17 atmospheric species between the LOTOS-EUROS and the Zeeman (12-hr forecast horizon). Data points represent a 1% random sample of the all points.

4.3. Vertical Evaluation of Forecasts

Zeeman is designed to forecast 3D concentration fields. The forecasts verified by far are solely on the ground level. It is essential to assess the error distribution in the vertical dimension as well. Figure 5 illustrates the vertical distribution of the correlation coefficient (R) across different lead times (6, 12, 18, and 24 hr) for six major pollutants. Additional metrics, including RMSE, NMB, and NME, are presented in Figures S14–S16 in Supporting Information S1. Generally, the error distribution remains consistent vertically and aligns with the concentration distribution, as shown in Figure S14 in Supporting Information S1. The vertical R values for NMVOC, $PM_{2.5}$, and PM_{10} are relatively high and stable, though they gradually decline with increasing lead time. For NH_3, R remains as high as 0.8 and stable across nearly all layers, except at the top layer, where it drops to near 0. Similar patterns of error variation are observed in NME and NMB. This behavior is attributed to extremely low concentration values in the upper layers, which can easily skew these metrics. For O_3, R remains stable across different lead times, with an increase observed in the upper layers due to elevated concentrations near the stratosphere. Its superior performance is further evident in the low errors and biases reflected in NME, NMB, and RMSE. In contrast, NO_2 exhibits a continuous decrease in R with altitude, corresponding to a rapid reduction in concentration due to photochemical reactions. This diminished performance highlights Zeeman's limitations in capturing this complex reaction accurately.

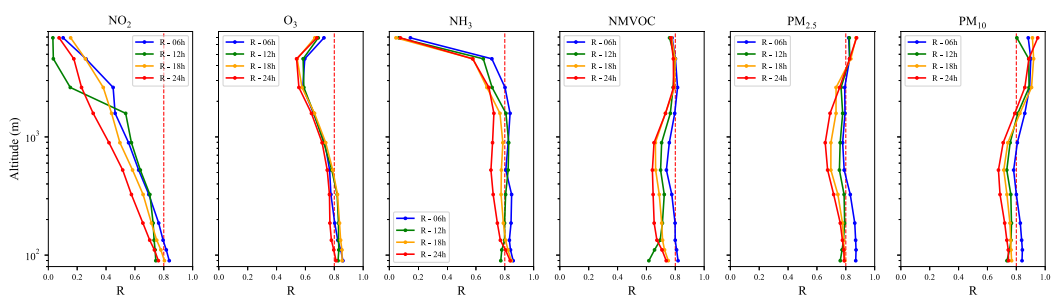

Figure 5. Vertical distribution of correlation coefficient (R) between Zeeman forecast and LOTOS-EUROS with the lead time of 6, 12, 18, 24 hr. All the forecasts start from 00:00 at each day on 2022.

19448007, 2026, 6, Downloaded from https://agupubs.onlinelibrary.wiley.com/doi/10.1029/2025GL117459 by Nanjing University Of Information Science & Technology, Wiley Online Library on [23/03/2026]. See the Terms and Conditions (https://onlinelibrary.wiley.com/terms-and-conditions) on Wiley Online Library for rules of use; OA articles are governed by the applicable Creative Commons License

19448007, 2026, 6, Downloaded from https://agupubs.onlinelibrary.wiley.com/doi/10.1029/2025GL117459 by Nanjing University Of Information Science & Technology, Wiley Online Library on [23/03/2026]. See the Terms and Conditions (https://onlinelibrary.wiley.com/terms-and-conditions) on Wiley Online Library for rules of use; OA articles are governed by the applicable Creative Commons License

5. Conclusion and Discussions

5.1. Conclusion

In this paper, we proposed a DL based regional atmospheric chemistry model–Zeeman. It facilitates the Swin Transformer architecture to capture interplay between concentration, emission and meteorological fields. Boundary conditions are also introduced to compensate for the outer pollution transport. Hourly simulations are made using an auto-regressive strategy. Performance of Zeeman simulations is evaluated. General performance of forecasts within 120 hr is evaluated. A stable performance for the majority of species, especially for six major pollutants, can be noticed. Meanwhile, A periodic pattern is found with respect to the different time of day. Experiments with random start hour and operational weather forecasts confirm that Zeeman isn't "drifting" or "exploding" as lead time increases; it is simply reacting to the varying difficulty of the atmospheric state. From the spatial view, high metrics can be noticed in O_3, PM simulations with correlation coefficient exceeding 0.85 over the majority of domain. For more active species, NO_2, NH_3 and NMVOC, an increase in certain duration in the daytime can be observed, which is associated with the diurnal variation of emission and meteorology. In the vertical dimension, errors are consistent with the concentration distribution. High correlation (around 0.8) in different layers can be found in most species.

5.2. Limitations and Future Work

While the current model represents a step forward, there are several areas where future improvements could be made. First, although a range of influential factors affecting air pollutant forecasting has been considered, additional data could further enhance the model's performance. For instance, incorporating the vertical diffusion coefficient and vertical air mass fluxes could improve the model's ability to capture vertical transport processes more accurately. The study domain is limited in the Netherlands for the limitation of computational resources. Additionally, the data set contains limited instances of extreme weather-emission combinations, which may constrain the model's capability to handle complex conditions effectively. In the future, more influential factors, a more extensive data set and a larger spatial domain would broaden the model's capability for operational applications.

Second, the absence of bidirectional chemistry-meteorology coupling represents a limitation of the current model, as it restricts the ability to capture the complex, two-way interactions between atmospheric chemistry and meteorology. These interactions, such as aerosol effects on radiation budgets (e.g., direct and indirect radiative forcing) as well as their feedback on chemical transport and reactions, are important for accurately simulating real-world atmospheric dynamics. While reproducing this interaction would require a fully coupled model, which is computationally expensive and demands greater GPU resources for convergence. In present, Zeeman can act as an offline coupler to meteorological models, leveraging external meteorological fields as inputs. To enhance its utility for air quality forecasting, we envision interfacing Zeeman with existing weather models (e.g., WRF, Pangu) to incorporate dynamic meteorological outputs while maintaining a modular structure.

Third, Zeeman is designed to serve as a fast, surrogate model that approximates LOTOS-EUROS's behavior while significantly reducing computational demands, and inaccuracies inherent in the LOTOS-EUROS may be carried over. To address this, assimilating observational data could refine Zeeman and lead to more accurate forecasts. Zeeman can be applied to perform efficient data assimilation, leveraging its computational speed to iteratively optimize emission estimates or high-frequency state optimization. With accurate emission estimates and concentrations, Zeeman can facilitate efficient optimization of pollutant concentrations, enabling rapid and reliable predictions of atmospheric composition.

Conflict of Interest

The authors declare no conflicts of interest relevant to this study.

Availability Statement

Zeeman was established on PyTorch, a Python based library for deep learning. In building and optimizing the backbones, Swin transformer is used and available at https://github.com/microsoft/Swin-Transformer. The user manual and inference code of Zeeman are public at a GitHub repository (https://github.com/xxcvvv/Zeeman) and

archived on Zenodo (Pang, 2026). Zeeman model and data set samples are archived on zenodo (Pang, 2025) for users to run the test runs.

Acknowledgments
This study was supported by the National Key Research and Development Program of China (Grants 2024YFE0113700 and 2025YFE0217100) and the National Natural Science Foundation of China (Grant 42475150).

References

Bi, K., Xie, L., Zhang, H., Chen, X., Gu, X., & Tian, Q. (2023). Accurate medium-range global weather forecasting with 3D neural networks. *Nature*, *619*(7970), 1–6. https://doi.org/10.1038/s41586-023-06185-3

Charlton-Perez, A. J., Dacre, H. F., Driscoll, S., Gray, S. L., Harvey, B., Harvey, N. J., et al. (2024). Do AI models produce better weather forecasts than physics-based models? A quantitative evaluation case study of storm Ciarán. *npj Climate and Atmospheric Science*, *7*(1), 1–11. https://doi.org/10.1038/s41612-024-00638-w

Chen, L., Zhong, X., Zhang, F., Cheng, Y., Xu, Y., Qi, Y., & Li, H. (2023). FuXi: A cascade machine learning forecasting system for 15-day global weather forecast. *npj Climate and Atmospheric Science*, *6*(1), 1–11. https://doi.org/10.1038/s41612-023-00512-1

Cheng, M., Fang, F., Navon, I. M., Zheng, J., Tang, X., Zhu, J., & Pain, C. (2022). Spatio-temporal hourly and daily ozone forecasting in China using a hybrid machine learning model: Autoencoder and generative adversarial networks. *Journal of Advances in Modeling Earth Systems*, *14*(3), e2021MS002806. https://doi.org/10.1029/2021MS002806

Colette, A., Collin, G., Besson, F., Blot, E., Guidard, V., Meleux, F., et al. (2024). Copernicus atmosphere monitoring service–Regional air quality production system v1.0 [preprint]. *EGUsphere*, 1–92. https://doi.org/10.5194/egusphere-2024-3744

de Burgh-Day, C. O., & Leeuwenburg, T. (2023). Machine learning for numerical weather and climate modelling: A review. *Geoscientific Model Development*, *16*(22), 6433–6477. https://doi.org/10.5194/gmd-16-6433-2023

Feng, X., Lin, H., Fu, T.-M., Sulprizio, M. P., Zhuang, J., Jacob, D. J., et al. (2021). WRF-GC (v2.0): Online two-way coupling of WRF (v3.9.1.1) and GEOS-chem (v12.7.2) for modeling regional atmospheric chemistry–meteorology interactions. *Geoscientific Model Development*, *14*(6), 3741–3768. https://doi.org/10.5194/gmd-14-3741-2021

Gao, C., Zhang, X., Xiu, A., Tong, Q., Zhao, H., Zhang, S., et al. (2024). Intercomparison of multiple two-way coupled meteorology and air quality models (WRF v4.1.1–CMAQ v5.3.1, WRF–chem v4.1.1, and WRF v3.7.1–CHIMERE v2020r1) in eastern China. *Geoscientific Model Development*, *17*(6), 2471–2492. https://doi.org/10.5194/gmd-17-2471-2024

George, C., Ammann, M., D'Anna, B., Donaldson, D. J., & Nizkorodov, S. A. (2015). Heterogeneous photochemistry in the atmosphere. *Chemical Reviews*, *115*(10), 4218–4258. https://doi.org/10.1021/cr500648z

Grell, G., & Baklanov, A. (2011). Integrated modeling for forecasting weather and air quality: A call for fully coupled approaches. *Atmospheric Environment*, *45*(38), 6845–6851. https://doi.org/10.1016/j.atmosenv.2011.01.017

Kuenen, J., Dellaert, S., Visschedijk, A., Jalkanen, J.-P., Super, I., & Denier van der Gon, H. (2022). CAMS-REG-v4: A state-of-the-art high-resolution European emission inventory for air quality modelling. *Earth System Science Data*, *14*(2), 491–515. https://doi.org/10.5194/essd-14-491-2022

Kuenen, J., Dellaert, S., Visschedijk, A., Jukka-Pekka, J., Super, I., & Gon Denier van der, H. (2021). Copernicus atmosphere monitoring service regional emissions version 4.2 (CAMS-REG-v4.2) [Dataset]. *ECCAD: Copernicus Atmosphere Monitoring Service*. https://doi.org/10.24380/0vzb-a387

Lam, R., Sanchez-Gonzalez, A., Willson, M., Wirnsberger, P., Fortunato, M., Alet, F., et al. (2023). Learning skillful medium-range global weather forecasting. *Science*, eadi2336. https://doi.org/10.1126/science.adi2336

Li, S., Wang, S., Wu, Q., Zhang, Y., Ouyang, D., Zheng, H., et al. (2023). Emission trends of air pollutants and CO_2 in China from 2005 to 2021. *Earth System Science Data*, *15*(6), 2279–2294. https://doi.org/10.5194/essd-15-2279-2023

Li, S., Zhao, Y., Varma, R., Salpekar, O., Noordhuis, P., Li, T., et al. (2020). PyTorch distributed: Experiences on accelerating data parallel training (No. arXiv:2006.15704). *arXiv*. https://doi.org/10.48550/arXiv.2006.15704

Li, Y., Han, W., Li, H., Duan, W., Chen, L., Zhong, X., et al. (2024). FuXi-En4DVar: An assimilation system based on machine learning weather forecasting model ensuring physical constraints. *Geophysical Research Letters*, *51*(22), e2024GL111136. https://doi.org/10.1029/2024GL111136

Liu, Z., Hu, H., Lin, Y., Yao, Z., Xie, Z., Wei, Y., et al. (2022). Swin transformer V2: Scaling up capacity and resolution. In *Proceedings of the IEEE/CVF conference on computer vision and pattern recognition (pp. 12009–12019)*.

Liu, Z., Lin, Y., Cao, Y., Hu, H., Wei, Y., Zhang, Z., et al. (2021). Swin transformer: Hierarchical vision transformer using shifted windows (No. arXiv:2103.14030). *arXiv*. https://doi.org/10.48550/arXiv.2103.14030

Loshchilov, I., & Hutter, F. (2019). Decoupled weight decay regularization (No. arXiv:1711.05101). *arXiv*. https://doi.org/10.48550/arXiv.1711.05101

Lu, B., Liu, C., Meng, X., Zhang, Z., Herrmann, H., & Li, X. (2023). High-resolution mapping of regional NMVOCs using the fast space-time light gradient boosting machine (LightGBM). *Journal of Geophysical Research: Atmospheres*, *128*(22), e2023JD039591. https://doi.org/10.1029/2023JD039591

Lu, X., Zhang, L., & Shen, L. (2019). Meteorology and climate influences on tropospheric ozone: A review of natural sources, chemistry, and transport patterns. *Current Pollution Reports*, *5*(4), 238–260. https://doi.org/10.1007/s40726-019-00118-3

Ma, P., Quan, J., Jia, X., Liao, Z., Wang, Q., Cheng, Z., et al. (2021). Effects of ozone and relative humidity in secondary inorganic aerosol formation during haze events in Beijing, China. *Atmospheric Research*, *264*, 105855. https://doi.org/10.1016/j.atmosres.2021.105855

Manders, A. M. M., Builtjes, P. J. H., Curier, L., Denier van der Gon, H. A. C., Hendriks, C., Jonkers, S., et al. (2017). Curriculum vitae of the LOTOS–EUROS (v2.0) chemistry transport model. *Geoscientific Model Development*, *10*(11), 4145–4173. https://doi.org/10.5194/gmd-10-4145-2017

Marécal, V., Peuch, V.-H., Andersson, C., Andersson, S., Arteta, J., Beekmann, M., et al. (2015). A regional air quality forecasting system over Europe: The MACC-II daily ensemble production. *Geoscientific Model Development*, *8*(9), 2777–2813. https://doi.org/10.5194/gmd-8-2777-2015

Méndez, M., Merayo, M. G., & Núñez, M. (2023). Machine learning algorithms to forecast air quality: A survey. *Artificial Intelligence Review*, *56*(9), 10031–10066. https://doi.org/10.1007/s10462-023-10424-4

Mu, Q., Shiraiwa, M., Octaviani, M., Ma, N., Ding, A., Su, H., et al. (2018). Temperature effect on phase state and reactivity controls atmospheric multiphase chemistry and transport of PAHs. *Science Advances*, *4*(3), eaap7314. https://doi.org/10.1126/sciadv.aap7314

Pang, M. (2025). Model and samples for "Zeeman: A Deep Learning Regional Atmospheric Chemistry Transport Model" [Collection]. *Zenodo*. https://doi.org/10.5281/zenodo.15162161

Pang, M. (2026). Xxcvvv/Zeeman: Zeeman v1.0 [Software]. *Zenodo*. https://doi.org/10.5281/zenodo.18462260

19448007, 2026, 6, Downloaded from https://agupubs.onlinelibrary.wiley.com/doi/10.1029/2025GL117459 by Nanjing University Of Information Science & Technology, Wiley Online Library on [23/03/2026]. See the Terms and Conditions (https://onlinelibrary.wiley.com/terms-and-conditions) on Wiley Online Library for rules of use; OA articles are governed by the applicable Creative Commons License

Peng, J., Hu, M., Shang, D., Wu, Z., Du, Z., Tan, T., et al. (2021). Explosive secondary aerosol formation during severe haze in the North China Plain. *Environmental Science & Technology*, *55*(4), 2189–2207. https://doi.org/10.1021/acs.est.0c07204

Peuch, V.-H., Engelen, R., Rixen, M., Dee, D., Flemming, J., Suttie, M., et al. (2022). The Copernicus atmosphere monitoring service: From research to operations. *Bulletin America Meteorology Social*, *103*(12), E2650–E2668. https://doi.org/10.1175/BAMS-D-21-0314.1

Qu, K., Yan, Y., Wang, X., Jin, X., Vrekoussis, M., Kanakidou, M., et al. (2024). The effect of cross-regional transport on ozone and particulate matter pollution in China: A review of methodology and current knowledge. *Science of the Total Environment*, *947*, 174196. https://doi.org/10.1016/j.scitotenv.2024.174196

Qu, Y., Voulgarakis, A., Wang, T., Kasoar, M., Wells, C., Yuan, C., et al. (2021). A study of the effect of aerosols on surface ozone through meteorology feedbacks over China. *Atmospheric Chemistry and Physics*, *21*(7), 5705–5718. https://doi.org/10.5194/acp-21-5705-2021

Raes, F., Liao, H., Chen, W.-T., & Seinfeld, J. H. (2010). Atmospheric chemistry-climate feedbacks. *Journal of Geophysical Research*, *115*(D12). https://doi.org/10.1029/2009JD013300

Skoulidou, I., Koukouli, M.-E., Manders, A., Segers, A., Karagkiozidis, D., Gratsea, M., et al. (2021). Evaluation of the LOTOS-EUROS NO_2 simulations using ground-based measurements and S5P/TROPOMI observations over Greece. *Atmospheric Chemistry and Physics*, *21*(7), 5269–5288. https://doi.org/10.5194/acp-21-5269-2021

Sokhi, R. S., Moussiopoulos, N., Baklanov, A., Bartzis, J., Coll, I., Finardi, S., et al. (2022). Advances in air quality research – Current and emerging challenges. *Atmospheric Chemistry and Physics*, *22*(7), 4615–4703. https://doi.org/10.5194/acp-22-4615-2022

Su, H., Cheng, Y., & Pöschl, U. (2020). New multiphase chemical processes influencing atmospheric aerosols, air quality, and climate in the Anthropocene. *Accounts of Chemical Research*, *53*(10), 2034–2043. https://doi.org/10.1021/acs.accounts.0c00246

Tang, D., Zhan, Y., & Yang, F. (2024). A review of machine learning for modeling air quality: Overlooked but important issues. *Atmospheric Research*, *300*, 107261. https://doi.org/10.1016/j.atmosres.2024.107261

Timmermans, R., Kranenburg, R., Manders, A., Hendriks, C., Segers, A., Dammers, E., et al. (2017). Source apportionment of $PM_{2.5}$ across China using LOTOS-EUROS. *Atmospheric Environment*, *164*, 370–386. https://doi.org/10.1016/j.atmosenv.2017.06.003

Timmermans, R., van Pinxteren, D., Kranenburg, R., Hendriks, C., Fomba, K. W., Herrmann, H., & Schaap, M. (2022). Evaluation of modelled LOTOS-EUROS with observational based PM10 source attribution. *Atmospheric Environment X*, *14*, 100173. https://doi.org/10.1016/j.aeaoa.2022.100173

TNO. (2025). Source code and user guidance of LOTOS-EUROS [Software]. *TNO*. https://airqualitymodeling.tno.nl/publish/pages/3175/lotos-euros_user-guide_v2-2-002_1.pdf

To, D., Quinting, J., Hoshyaripour, G. A., Götz, M., Streit, A., & Debus, C. (2024). Architectural insights into and training methodology optimization of Pangu-Weather. *Geoscientific Model Development*, *17*(23), 8873–8884. https://doi.org/10.5194/gmd-17-8873-2024

Wang, J., Ge, B., Kong, L., Chen, X., Li, J., Lu, K., et al. (2024). Quantitative decoupling analysis for assessing the meteorological, emission, and chemical influences on fine particle pollution. *Journal of Advances in Modeling Earth Systems*, *16*(11), e2024MS004261. https://doi.org/10.1029/2024MS004261

Wang, W., Ren, K., Duan, B., Zhu, J., Li, X., Ni, W., et al. (2024). A four-dimensional variational constrained neural network-based data assimilation method. *Journal of Advances in Modeling Earth Systems*, *16*(1), e2023MS003687. https://doi.org/10.1029/2023ms003687

Xiao, Q., Zheng, Y., Geng, G., Chen, C., Huang, X., Che, H., et al. (2021). Separating emission and meteorological contributions to long-term $PM_{2.5}$ trends over eastern China during 2000–2018. *Atmospheric Chemistry and Physics*, *21*(12), 9475–9496. https://doi.org/10.5194/acp-21-9475-2021

Yu, S., & Ma, J. (2021). Deep learning for geophysics: Current and future trends. *Reviews of Geophysics*, *59*(3), e2021RG000742. https://doi.org/10.1029/2021RG000742

Zhang, B., Rong, Y., Yong, R., Qin, D., Li, M., Zou, G., & Pan, J. (2022). Deep learning for air pollutant concentration prediction: A review. *Atmospheric Environment*, *290*, 119347. https://doi.org/10.1016/j.atmosenv.2022.119347

Zhang, B., Zhang, H., Zhao, G., & Lian, J. (2020). Constructing a PM2.5 concentration prediction model by combining auto-encoder with Bi-LSTM neural networks. *Environmental Modelling & Software*, *124*, 104600. https://doi.org/10.1016/j.envsoft.2019.104600

Zhang, C., Jiang, Z., Liu, M., Dong, Y., & Li, J. (2023). Relationship between summer time near-surface ozone concentration and planetary boundary layer height in Beijing. *Atmospheric Research*, *293*, 106892. https://doi.org/10.1016/j.atmosres.2023.106892

Zhang, Y. (2008). Online-coupled meteorology and chemistry models: History, current status, and outlook. *Atmospheric Chemistry and Physics*, *8*(11), 2895–2932. https://doi.org/10.5194/acp-8-2895-2008

Zhang, Y., Bocquet, M., Mallet, V., Seigneur, C., & Baklanov, A. (2012). Real-time air quality forecasting, part I: History, techniques, and current status. *Atmospheric Environment*, *60*, 632–655. https://doi.org/10.1016/j.atmosenv.2012.06.031

Zhong, X., Chen, L., Li, H., Liu, J., Fan, X., Feng, J., et al. (2024). FuXi-ENS: A machine learning model for medium-range ensemble weather forecasting (No. arXiv:2405.05925). *arXiv*. https://doi.org/10.48550/arXiv.2405.05925

Zhu, T., Tang, M., Gao, M., Bi, X., Cao, J., Che, H., et al. (2023). Recent progress in atmospheric chemistry research in China: Establishing a theoretical framework for the "Air Pollution Complex". *Advances in Atmospheric Sciences*, *40*(8), 1339–1361. https://doi.org/10.1007/s00376-023-2379-0

19448007, 2026, 6, Downloaded from https://agupubs.onlinelibrary.wiley.com/doi/10.1029/2025GL117459 by Nanjing University Of Information Science & Technology, Wiley Online Library on [23/03/2026]. See the Terms and Conditions (https://onlinelibrary.wiley.com/terms-and-conditions) on Wiley Online Library for rules of use; OA articles are governed by the applicable Creative Commons License